# Vibronic effects in the absorption spectra of strontium phenoxide, SrOPh, and its deuterated version, SrOPh-$d_5$

..., Paweł Wójcik, ...

March 26, 2025

## 1 Introduction

This document presents simulation of the absorption spectra of strontium phenoxide and its deuterated version: SrOPh, SrOPh-$d_5$. Both molecules belong of the family of second-group metal organic-mono-oxides, which are characterized by an alkali-atom-like spectrum induced by the presence of a single unpaired electron localized at the metal atom. The molecular ground state $\tilde{X}^2A_1$ corresponds to the hydrogen-atom-like ($5s^1$) $^2$S state of Rb. The pair of molecular states, $\tilde{A}^2B_2$ and $\tilde{B}^2B_1$, corresponds to two of the triply-degenerate ($5p^1$) $^2$P states, where the degeneracy is lifted by the lowered symmetry of the molecule. The $\tilde{C}^2A_1$ state corresponds to the third component of $^2P$ state, which would extend towards the phenoxide ligand, and as such it is more mixed and shows a larger energy gap.

All four states are characterized by very similar equilibrium structures and very similar potential energy surfaces, which results in almost no changes to the vibrational state during radiative decay of the excited states.

The lowest frequency modes are vibrations of the M-O-C group. In case of SrOPh, the three lowest frequency modes, in order are: the in-plane M-O-C bend, $\nu_{33}(b_2)$, the out-of-plane M-O-C bend, $\nu_{22}(b_1)$, and the M-O stretch, $\nu_{12}(a_1)$. There is at least one more set of higher frequency modes that has a significant component along each of these three motions. The deuterated molecule shares similar traits.

Out of these three types of motion, the best studied one is the M-O stretch. The reason behind it lies in the extensively studied fluorescence spectrum of the vibrationless $\tilde{A}$ or $\tilde{B}$ states. Such spectra shows progressions in the M-O stretching modes which are attributed to the changes in the M-O bond length between the electronic states; the most prominent, although very small, geometrical relaxation.

This work focuses on the states that lie above the vibrational ground state of the $\tilde{A}$ state, all the way up in the energy range past the $\tilde{B}$ state, a region spanning about 700 $cm^{-1}$. In this region, the M-O stretching modes remain

highly relevant and prominent, however, it is also the range where the M-O-C bending modes exhibit its significance as the carriers of the vibronic couplings.

The presence of the vibronic couplings stresses that the description of the vibronic states as products of an electronic state and a vibrational state is no longer valid. The vibronic states, which are the eigenstates of the molecular Hamiltonian, show mixing of various electronic states used in the zeroth-order model described above. This work simulates the vibronic states using the Köppel-Domcke-Cederbaum (KDC) Hamiltonian and discusses the consequences of the mixing on the fluorescence spectra and prospects of optical cycling.

## 2 Methods

The methods used in this work were recently successful in simulations of vibronic effects in other molecules, in particular for YbOH, CaOH, SrOH, RaOH, $SrOCH_3$, $SrNH_2$, $NO_3$, benzene cation, $O_3$, and pyrazine.[1–8] The specific shape of the quantum chemistry models and the vibronic Hamiltonian used in this work is described below.

The electronic structure calculations use the coupled-cluster (CC) based methods.[9] In particular we use the electron attachment flavor of the equation-of-motion extension of CC truncated to single and double substitutions (EOM-EA-CCSD).[10–14]

We compute the vertical excitation energies $E^{(\alpha)}$ using composite schemes involving basis set extrapolation and use of EOM-CC truncated to include full single, double, and perturbative triple excitations (EOM-CCSD*), where the highest level of theory was especially needed for the $\tilde{C}$ state.[15] All CC calculations were carried out in CFOUR and Q-Chem.[16–19] We did not invoke the frozen-core approximation — all electrons were included in the correlated calculations.

The vibronic simulations use the KDC Hamiltonian.[20–22] The KDC Hamiltonian is designed for use in a basis of diabatic states which for which we use the definition of Ichino, Gauss, and Stanton.[23]

The KDC Hamiltonian (expanded in the dimensionless normal coordinates of the ground state)

$$H_{KDC} = H_0\mathbf{1} + \begin{bmatrix} V^{(\tilde{A})} & V^{(\tilde{A}\tilde{B})} & V^{(\tilde{A}\tilde{C})} \\ V^{(\tilde{B}\tilde{A})} & V^{(\tilde{B})} & V^{(\tilde{B}\tilde{C})} \\ V^{(\tilde{C}\tilde{A})} & V^{(\tilde{C}\tilde{B})} & V^{(\tilde{C})} \end{bmatrix}, \tag{1}$$

consists of the diagonal harmonic terms

$$H_0 = -\frac{1}{2}\sum_{i=1}^{N_{nm}} \omega_i \left(\partial_{Q_i}^2 + Q_i^2\right), \tag{2}$$

the diagonal diabatic potential terms

$$V^{(\alpha)} = E^{(\alpha)} + \sum_{i=1}^{N_{nm}} \kappa_i^{(\alpha)} Q_i \tag{3}$$

and the off-diagonal, diabatic coupling terms

$$V^{(\alpha\beta)} = \sum_{i \in \{\text{coupling modes}\}} \lambda_i^{(\alpha\beta)} Q_i. \tag{4}$$

$N_{nm}$ is the number of normal modes included in the model. $\mathbf{1}$ is a $3 \times 3$ identity matrix. $\omega_i$ is the ground state harmonic frequency of the normal mode $i$. $Q_i$ is a dimensionless normal coordinate. $E^{(\alpha)}$ is the vertical excitation energy of the electronic state $\alpha$. $\kappa_i^{(\alpha)}$ is energy gradient of state $\alpha$ along the dimensionless normal mode $i$. $\lambda_i^{(\alpha\beta)}$ is the linear diabatic coupling constant between states $\alpha$ and $\beta$ along normal mode $i$.

Using definition of (quasi)-diabatic states given by Ichino, Gauss, and Stanton, the linear diabatic coupling constants, $\lambda_i^{(\alpha\beta)}$, were computed *ab initio*.[23] Along fully symmetric modes, where the diabatic potential coincides with the adiabatic potential, the linear expansion coefficients $\kappa_i^{(\alpha)}$ were calculated *ab initio* using the EOM-CCSD analytic gradients, while along the non-fully-symmetric modes these coefficients vanish as all states were found to have planar $C_{2v}$ symmetry.[24]

We simulate the vibronic spectrum with the XSIM program.[25] The vibronic simulations used 15 basis set functions per vibrational mode and 2000 Lanczos iterations.

The ground-state geometry was optimized using EOM-EA-CCSD. The SrOPh geometry was optimized using EOM-EA-CCSD/cc-PVDZ[H,C,O]/cc-pwCVDZ-DK2[Sr]. The calculations of the harmonic frequencies, potential expansion coefficients $\kappa$ and linear diabatic couplings $\lambda$, were carried out at the same level of theory.

The calculation of the vertical excitation energies $E^{(\alpha)}$ were carried out using a composite scheme: the EOM-EA-CCSD energies were calculated using a series of basis sets and extrapolated to the complete basis set (CBS) limit. The higher correlation effect was added by calculating the difference between the EOM-EA-CCSD* and EOM-EA-CCSD energies, and the difference was applied to the energies as a triples correction. The spin-orbit couplings (SOC) were calculated between the $\tilde{X}$, $\tilde{A}$, $\tilde{B}$, and $\tilde{C}$ states, the SOC Hamiltonian was constructed and diagonalized (see SI of Ref. [26] for details) to yield the final values of the vertical excitation energies.

In the multistate and multimode KDC Hamiltonian three excited electronic states are coupled: $\tilde{A}$, $\tilde{B}$, and $\tilde{C}$. A varying number of normal modes is included throughout the simulations in order to observe the impact of various modes on the vibronic spectrum. All 33 normal modes cannot be included in the simulation as this leads to numerically intractable problem. The parameters

| $E^{(\alpha)}$ | aug-cc-pwCVDZ | aug-cc-pwCVTZ | aug-cc-pwCVQZ | CBS |
|---|---|---|---|---|
| $\tilde{A}$ | 14288 | 14501 | 14512 | 14520 |
| $\tilde{B}$ | +195 | +169 | +167 | +165 |
| $\tilde{C}$ | +1966 | +1668 | +1615 | +1577 |

Table 1: Vertical excitation energies for the SrOPh in $cm^{-1}$. The first row presents the energy of the $\tilde{A}$ state while the rows for the $\tilde{B}$ and $\tilde{C}$ states show the energy gap above the $\tilde{A}$ state. Calculated using EOM-EA-CCSD and correlating all electrons, with pseudopotential for the core Sr electrons ECP28MDF.

| $E^{(\alpha)}$ | EOM-CCSD/CBS | $\Delta$EOM-CCSD$^*$ | SOC | final |
|---|---|---|---|---|
| $\tilde{A}$ | 14520 | +40 | -73 | 14487 |
| $\tilde{B}$ | 14685 | +24 | +53 | 14762 |
| $\tilde{C}$ | 16097 | -209 | +10 | 15898 |

Table 2: Vertical excitation energies for the SrOPh in $cm^{-1}$. Corrections due to the triples correlation ($\Delta$EOM-EA-CCSD$^*$) and spin-orbit couplings.

of the KDC Hamiltonian are expanded around the ground state's equilibrium geometry.

The molecular orientation and normal mode labels follow the Mulliken's convention.[27] The molecule is oriented in the $yz$-plane with the symmetry axis along the $z$ axis. The normal modes are ordered first by their symmetry: $a_1$, $a_2$, $b_1$, $b_2$. Within each symmetry block the modes are ordered by their harmonic frequencies in a decreasing order. Out of the 33 normal modes of the molecule 12 transforms with $a_1$ irrep, 3 with $a_2$, 7 with $b_1$, and 11 with $b_2$.

# 3 Results

This section opens with description of the parameters that enter the KDC Hamiltonian and moves to the description of the simulated spectra focusing on the appearance of the vibronic features.

## 3.1 Parameters of the KDC Hamiltonian

The parameters of the KDC Hamiltonian, Eq. (1), are expanded around the optimized geometry of the $\tilde{X}$ state. This section first presents the vertical excitation energies, then the harmonic frequencies, and the couplings.

The vertical excitation energies were calculated using a composite scheme discussed in the Sec. 2. Table 1 lists the vertical excitation energies and their CBS limit. The main observation is that the quadruple-$\zeta$-quality basis is within 10 $cm^{-1}$ from the CBS limit for the $\tilde{A}$ and $\tilde{B}$ state and about five times as far for the $\tilde{C}$ state. Table 2 lists the corrections due to higher correlation effects and the SOCs. The triples correction are of the order of tens of wavenumbers for

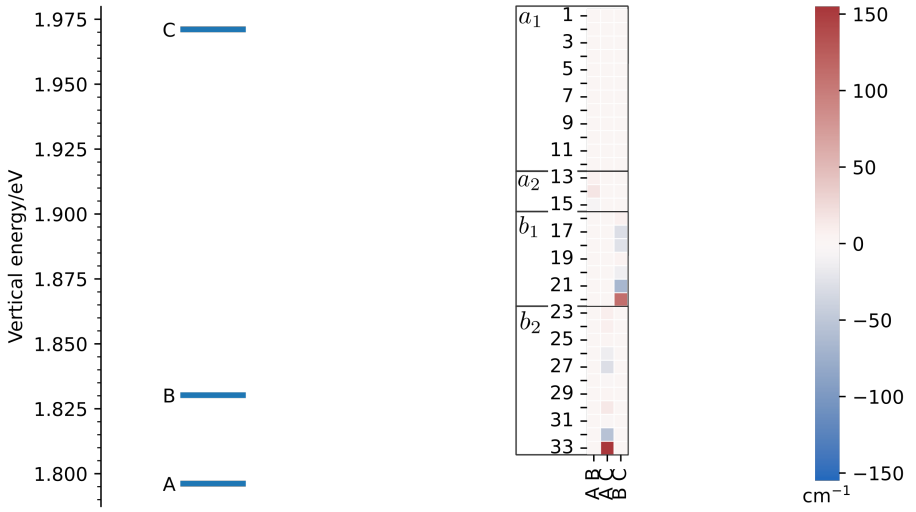


Figure 1: Left: vertical excitation energies, i.e., $E^{(\alpha)}$s from Eq. (3). Right: Linear diabatic couplings, i.e., $\lambda$s from Eq. (4), for SrOPh.

the $\tilde{A}$ and $\tilde{B}$ states, and again a much larger for the $\tilde{C}$ state. The SOCs repel the $\tilde{A}$ and $\tilde{B}$ state by more than 100 cm$^{-1}$. The SOCs do not shift the energy of the $\tilde{C}$ state by much, however, the $\tilde{C}$ state might interact more strongly with the higher states that are not included in this model. The right-most column of Table 2 shows the final values of this composite scheme, these values are also plotted on figure 1.

All remaining parameters of the model are expanded in the basis of normal modes of the ground state. The harmonic frequency of the fully symmetric stretch, $\nu_{12}(a_1)$ is 239 cm$^{-1}$. The harmonic frequencies of the non-fully-symmetric modes are: 65 cm$^{-1}$ for the in-plane Sr-O-C bend, $\nu_{33}(b_2)$, and 84 cm$^{-1}$ for the out-of-plane Sr-O-C bend, $\nu_{22}(b_1)$. The next mode, in the order of increasing frequency, $\nu_{21}(b_1)$, has the frequency 273 cm$^{-1}$ and is also largely an out-of-plane Sr-O-C bend. These four modes, their combinations, and their couplings produce most of the vibronic features in the region between and close to the $\tilde{A}$, and $\tilde{B}$ states, which in this model are separated by the vertical gap of 275 cm$^{-1}$.

Figure 1 presents the structure of the linear diabatic couplings for SrOPh. The couplings between $\tilde{A}$ and $\tilde{C}$ states (middle column) are the strongest along the in-plane Sr-O-C bending modes, these are the modes displacing the Sr and O atoms into the electronic density of the unpaired electron in the $\tilde{A}$ state. Similarly, the $\tilde{B}$ and $\tilde{C}$ states couple along the out-of-plane Sr-O-C modes. The linear vibronic coupling constants between $\tilde{A}$ and $\tilde{B}$ states are vanishingly small. The coupling between these two, closely-lying states appear in this model in second-order, e.g., through a vibronically active combination modes.

## 3.2 Vibronic simulation results

The role of the vibronic effects in the simulated spectrum is best presented when the vibronic spectrum is compared against the simulation which does not include the vibronic couplings, see figure 2.

The uncoupled spectrum is typical for a laser-coolable molecule. The most prominent peak in the spectrum corresponds to the electronic transition which does not change the vibrational state. The key transitions which change the vibrational state excite the $\nu_{12}$ mode, i.e., the mode with a significant Sr-O stretching component. The progression in $\nu_{12}$ is present both in the $\tilde{A}$ and $\tilde{B}$ states, but the peaks' intensities make less than 10 % of the 0-0 peak's intensity. Both simulations also show the small $\nu_{11}(a_1)$ peak close to the 600 cm$^{-1}$ mark, that corresponds to the second, lowest-frequency mode with the Sr-O stretching component. This is a complete description of the major features of the spectrum visible up to about the first 600 cm$^{-1}$. The simulation which neglects the vibronic couplings reproduces these features very well. A closer inspection of the spectrum, however, reveals an important role of the vibronic couplings.

The role of figure 3 is to bring focus to the finer features of the vibronic spectrum; features which are missing in the uncoupled simulation. This spectrum reveals a massive enhancement in the number of vibronic states that are weakly allowed as a consequence of the vibronic effects. The KDC-Hamiltonian-based simulations reveal that there are two mechanisms leading to the appearance of these features: the direct and second-order vibronic couplings.

### 3.2.1 The direct coupling of the $\tilde{A}$ and $\tilde{B}$ states to the $\tilde{C}$ state

The first vibronic effect is an appearance of progressions directly resulting from the linear vibronic coupling model. Figure 4 helps in this discussion by presenting an assignment of the vibronic features of the fully *ab initio* simulated spectrum. The assignments appear as a Franck-Condon-type decoupled state labels, but these are only used to mark the leading terms in the otherwise mixed state. The linear vibronic couplings model used in this work is based on diabatic couplings between electronic states. These couplings appear between pairs of electronic states as expansion coefficients along non-fully-symmetric modes as presented on figure 1. Such modes are inactive in the uncoupled, i.e., Franck-Condon simulation. The couplings allow for mixing of electronic states along the coupling modes.

The lowest-energy progression of this type appears for the $\nu_{33}$ mode (in-plane Sr-O-C bending) and is labeled $^{\tilde{A}}33^n$ on figure 4. The symmetry of vibronic peaks in this progression changes between the symmetry of the "host", $\tilde{A}$ electronic state (for even number of quanta) and of the "coupled", $\tilde{C}$ electronic state (for odd number of quanta). This progression differs from a typical Franck-Condon progression in the peaks' intensity distribution. The intensities depend not only on the number of vibrational quanta but also on the energetic distance to the state which leaks the intensity.

Analogous progressions are also marked as $^{\tilde{A}}12^1 33^n$ and $^{\tilde{B}}22^n$ on figure 4.

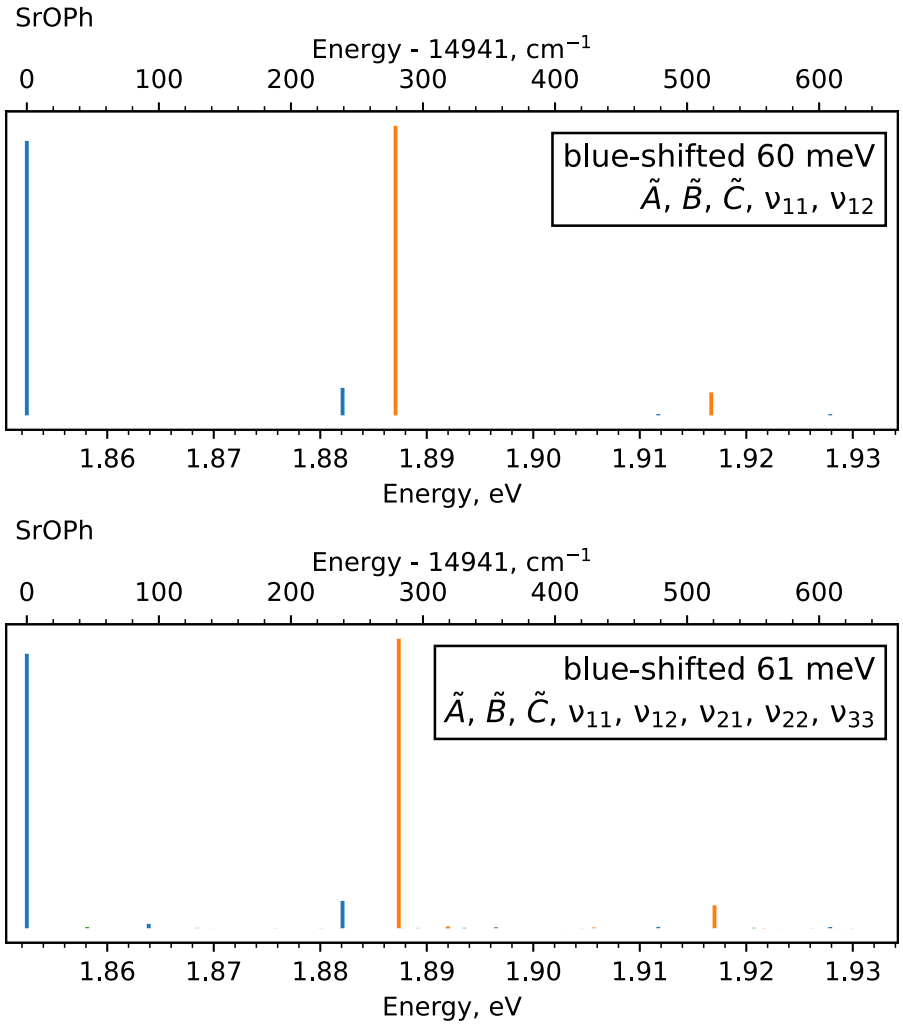


Figure 2: Simulated absorption spectrum of SrOPh. The top spectrum displays the no-couplings case (Franck-Condon simulation). Colors mark symmetry of the vibronic peaks: blue $B_2$, orange $B_1$, green $A_1$. The inset box marks the states and modes active in the simulation.

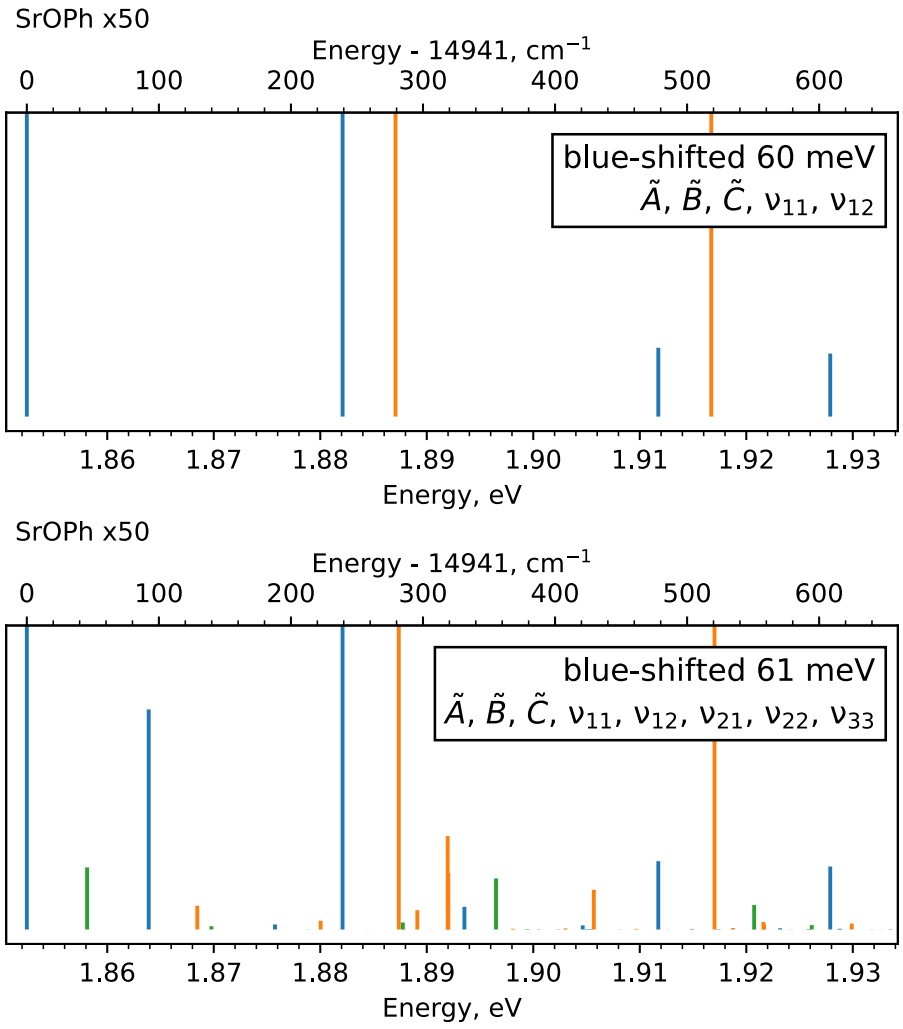


Figure 3: A blow-up version of figure 2.

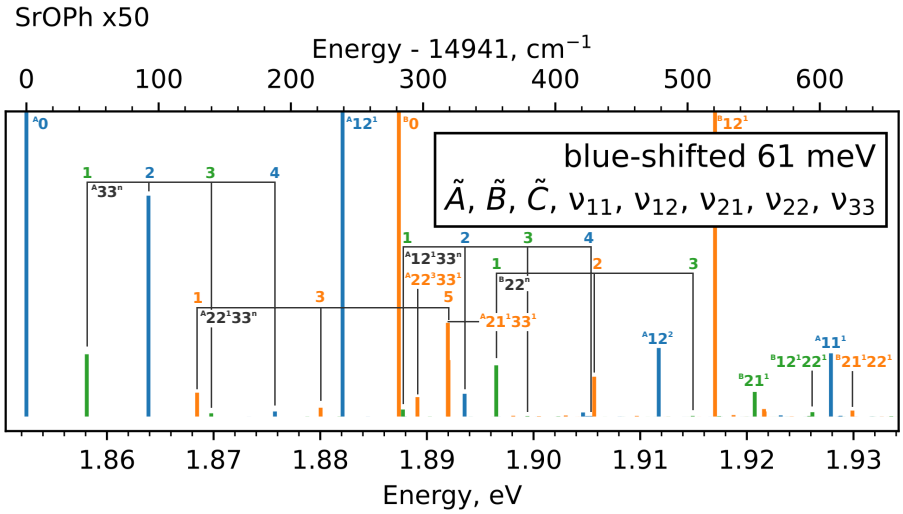


Figure 4: Simulated vibronic spectrum with annotations marking peak's assignments. The assignments corresponds to the leading term in the states which are mixed due to the vibronic couplings. Colors mark symmetry of the vibronic peaks: blue $B_2$, orange $B_1$, green $A_1$.

The latter one corresponds to the coupling of $\tilde{B}$ and $\tilde{C}$ states along the $\nu_{22}$ mode. Peaks ${}^{\tilde{B}}12^122^1$ and ${}^{\tilde{B}}21^1$ also appear through this mechanism, however, only the first peak of both series is visible in the figure 4.

### 3.2.2 Second-order coupling between $\tilde{A}$ and $\tilde{B}$ states

The progressions discussed above are expected as a result of the linear coupling model of the KDC Hamiltonian. New vibronic states appear as a consequence of significant couplings along non-fully-symmetric modes. Figure 1 shows that the couplings between the $\tilde{A}$ and $\tilde{B}$ states are almost vanishing compared to the coupling to the $\tilde{C}$ state. Despite the lack of a direct, or first-order, coupling, the $\tilde{A}$ and $\tilde{B}$ states couple by a second-order mechanism.

Symmetry of the $\tilde{A}$ and $\tilde{B}$ states requires that these two can only mix along modes of the $a_2$ symmetry. Figure 1 shows that for the lowest-frequency mode of this symmetry (mode $\nu_{15}(a_2)$ with harmonic frequency 426 cm$^{-1}$) the coupling is vanishingly small, making it unlikely to produce any significant features. There are however another type of modes that have the desired $a_2$ symmetry. These are the modes that appear as combinations of modes of $b_1$ and $b_2$ symmetry; these are the ones coupling $\tilde{B}$-$\tilde{C}$ and $\tilde{A}$-$\tilde{C}$ states, respectively, and these modes exhibit significant vibronic activity, as discussed earlier. We call the vibronic features appearing along such combination modes as the second-order effects.

The progression labelled as ${}^{\tilde{A}}22^133^n$ on figure 4 is the second-order effect.

This progression is built out of the $\nu_{33}$ (Sr-O-C in-plane bend) and $\nu_{22}$ (Sr-O-C out-of-plane bend) modes. These vibronic peaks are are bright by drawing the intensity from mixing with the $\tilde{B}$ state. Only odd number of excitations appear, as all of $^{\tilde{B}}22^{1}33^{2n}$ states have the $A_2$ symmetry which are dark in the 0K absorption spectrum. The peak individually labelled as $^{\tilde{A}}22^{3}33^{1}$ can also be viewed as the second peak in the unlabelled progression $^{\tilde{A}}22^{n}33^{1}$.

The coupling between the $\nu_{33}$ and $\nu_{22}$ modes is also interesting by comparison with the work on linear triatomics, like CaOH or YbOH. These two modes would be degenerate bends of the Sr-O-C part of the molecule if it was not for the symmetry-breaking phenol ring. In case of linear triatomics, the excited states of these bending modes can be expressed in a basis forming vibrational angular momentum. Such basis is often more convenient for discussion of angular momentum couplings.[28] Analogously, the $\tilde{A}$ and $\tilde{B}$ states would correlate to a degenerate pair in the linear molecule limit, however it was already noted that the angular momentum of the $\tilde{A}$ and $\tilde{B}$ states is largely quenched by the symmetry-breaking phenol ring.[29] Given this perspective, the coupling of the $\tilde{A}$ and $\tilde{B}$ states through the combined $\nu_{33}$ and $\nu_{22}$ modes can be correlated to the Renner-Teller coupling in linear molecules.

The second-order effect also displays the modulation in the relative feature intensities. The peak $^{\tilde{A}}22^{1}33^{1}$ is more intense than $^{\tilde{A}}22^{1}33^{3}$, where it seems like the vibrational overlap dominates over the intensity borrowing coming from mixing, while the $^{\tilde{A}}22^{3}33^{1}$ peak shows higher intensity than $^{\tilde{A}}22^{1}33^{3}$ likely due to the increased proximity to the very strong $^{\tilde{B}}0$ peak.

Another intense peak of the second-order type is the $^{\tilde{A}}21^{1}33^{1}$ one. The mode $\nu_{21}$ has a significant component of the Sr-O-C out-of-plane bend, similar to $\nu_{22}$. Despite the fact that the coupling along $\nu_{21}$ is weaker than the coupling along $\nu_{22}$, this peak is much more intense than the $^{\tilde{A}}22^{1}33^{1}$, a difference that is explored further in the next section.

### 3.2.3 Sensitivity of peak features on the parameters of the Hamiltonian

The discussion of the second-order vibronic effects highlights that the intensity of the vibronic features is strongly tied not only to the strength of the diabatic couplings but also to the gaps in the vertical excitation energy between the coupled states. As described in Sec. 3.1 the *ab inito* error estimate for the gap between the $\tilde{A}$ and $\tilde{B}$ states has to be at least a few tens of wavenumbers; and indeed the comparison against the experimental spectrum shows discrepancy of that order. To estimate the relevance of the vibronic structure findings, this section presents a study of the sensitivity of the vibronic peaks' character to the value of the gap between the $\tilde{A}$ and $\tilde{B}$ states.

We focus on the $^{\tilde{B}}0$ state and the two nearest vibronic peaks resulting from the second-order coupling to the $\tilde{A}$ state: the $^{\tilde{A}}22^{3}33^{1}$ and $^{\tilde{A}}21^{1}33^{1}$ states. These vibronic states are chosen as they draw the intensity from the $^{\tilde{B}}0$ and are energetically the closest, therefore these states are expected to show the

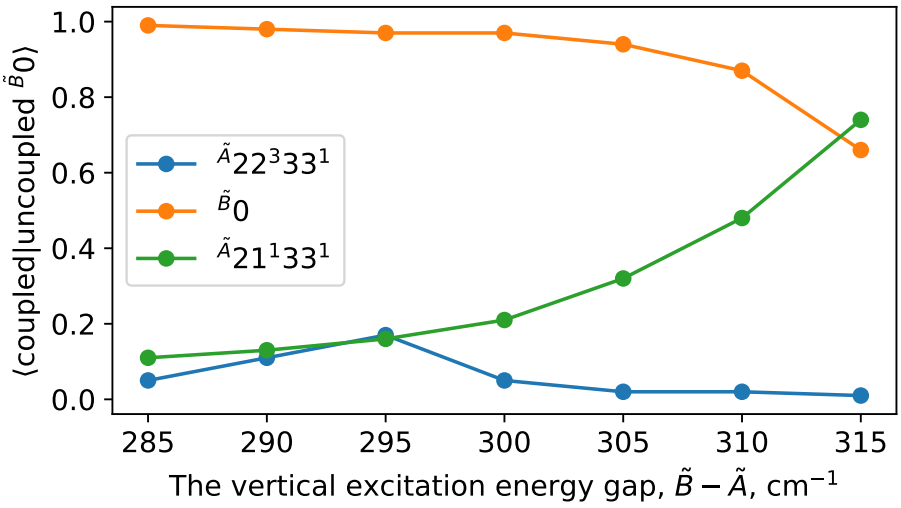


Figure 5: Dependents of the content of the uncoupled $^{\tilde{B}}0$ state on the vertical excitation energy gap between the $\tilde{A}$ and $\tilde{B}$ states for three states in the proximity of the $\tilde{B}$ state's origin.

strongest response to any changes in vertical excitation energy of the $\tilde{B}$ state.

Figure 5 presents changes to the character of the vibronic peaks as a function of the vertical gap between the $\tilde{A}$ and $\tilde{B}$ states. The gap is changed by increasing the vertical excitation energy of the $\tilde{B}$ state while keeping the $\tilde{A}$ state's position unchanged. The character of the vibronic state is measured as an overlap between the coupled state and the uncoupled, i.e., Franck-Condon, version of the $^{\tilde{B}}0$ state, the details of this procedure are described in Ref. [8].

The coupled $^{\tilde{B}}0$ state shows significant resemblance to its uncoupled version. The overlap value drops when the energetic spacing to another coupled state becomes significant. The curve for the $^{\tilde{A}}22^{3}33^{1}$ state shows that the coupling to the $^{\tilde{B}}0$ state results in a maximum mixing at the $\tilde{A}$-$\tilde{B}$ gap close to 295 cm$^{-1}$. A denser sampling in that region would likely reveal an even stronger mixing between the two states. The case of $^{\tilde{A}}21^{1}33^{1}$ state is an example of such stronger mixing, at the values close to 315 cm$^{-1}$ both states carry equal content of the $^{\tilde{B}}0$ state. The two top, right-most points on the figure should in fact already switch the colors as the character of the two states has already changed.

The example of coupling of $^{\tilde{B}}0$ to either $^{\tilde{A}}22^{3}33^{1}$ or $^{\tilde{A}}21^{1}33^{1}$ shows how the vibronic effects can lead to a very bright state leaking as much as half of its intensity to an otherwise dark state. The difference in the response of $^{\tilde{A}}22^{3}33^{1}$ and $^{\tilde{A}21^{1}33^{1}}$ to the position of the $^{\tilde{B}}0$ state shows that for some dark states the vibronic coupling can produce significant intensity borrowing even if the positions of the uncoupled states are relatively far apart (the $^{\tilde{A}}21^{1}33^{1}$

case), while for other states (the $^{\tilde{A}}22^{3}33^{1}$ case) the accidental degeneracy of the uncoupled states is needed in order to observe strong mixing.

### 3.2.4 Isotope substitution

The Sec. 3.2.3 discussed the importance of the value of the vertical energy gap between electronic states in the simulations of the vibronic effects. The gap changes of the order of tens of wavenumbers can result in profoundly different intensities of the peak spectra. Similar observation should apply to the response of the simulated spectrum to the changes in the frequencies of the uncoupled modes. Instead of considering a model in which these frequencies are shifted arbitrarily, this section considers the case of deuterated molecules.

Deuterated strontium phenoxide SrOPh-$d_5$ would be characterized by the same parameters as SrOPh, except for changes in the normal modes, effectively allowing to study, also experimentally, the response of the vibronic spectrum to the shifts in the positions of uncoupled vibrational states.

The changes of the normal modes of the strontium phenoxide due to deuteration are visualized on figure 6. The figure presents the matrix of inner products between the two sets of normal modes, also known as the Duschinsky rotation matrix. The columns and rows of the matrix additionally list the harmonic wavenumbers of the corresponding modes. The figure shows that the lowest frequency modes remain largely unchanged in the deuterated molecule and can still be identified as various displacements of the Sr-O-C group of atoms. The harmonic wavenumbers of the deuterated modes lower by about 5%. The medium-frequency modes change not only its frequencies but also its shape, however, none of these modes was significant for the simulations discussed earlier.

The main focus of this section is to view the changes in the vibronic spectra due to small changes in the positions of uncoupled states. As described in the previous paragraph deuteration of the molecule allows to achieve the exact effect.

With the changes of the normal modes, the expansion coefficients of the KDC Hamiltonian, Eqs. (4) and (3) change as well. Figure 7, presents the changed values and structure of the diabatic couplings. The key qualitative properties are preserved, i.e., strong coupling of $\tilde{A}$-$\tilde{C}$ states along $\nu_{33}$, strong coupling of $\tilde{B}$-$\tilde{C}$ states along $\nu_{22}$ and $\nu_{21}$, and vanishing couplings between $\tilde{A}$-$\tilde{B}$. Quantitatively, the couplings strengths become a little weaker. Overall, the consequence of this change is that the comparison between the deuterated and undeuterated molecules probes a few more parameters of the KDC Hamiltonian than only the position of uncoupled vibronic states.

The simulated spectrum of the deuterated molecule is presented on figure 8. The progressions discussed in Sec. 3.2.1 remain largely unchanged upon the deuteration with the only difference appearing due to the small frequency shifts of the deuterated modes. There are however two states that respond to the deuteration far stronger, these are the same sates as discussed in Sec. 3.2.3, the $^{\tilde{A}}22^{3}33^{1}$ and $^{\tilde{A}}21^{1}33^{1}$. For both of them the small change in the frequency is met with a significant increase in their intensity, as the shift moves both sates

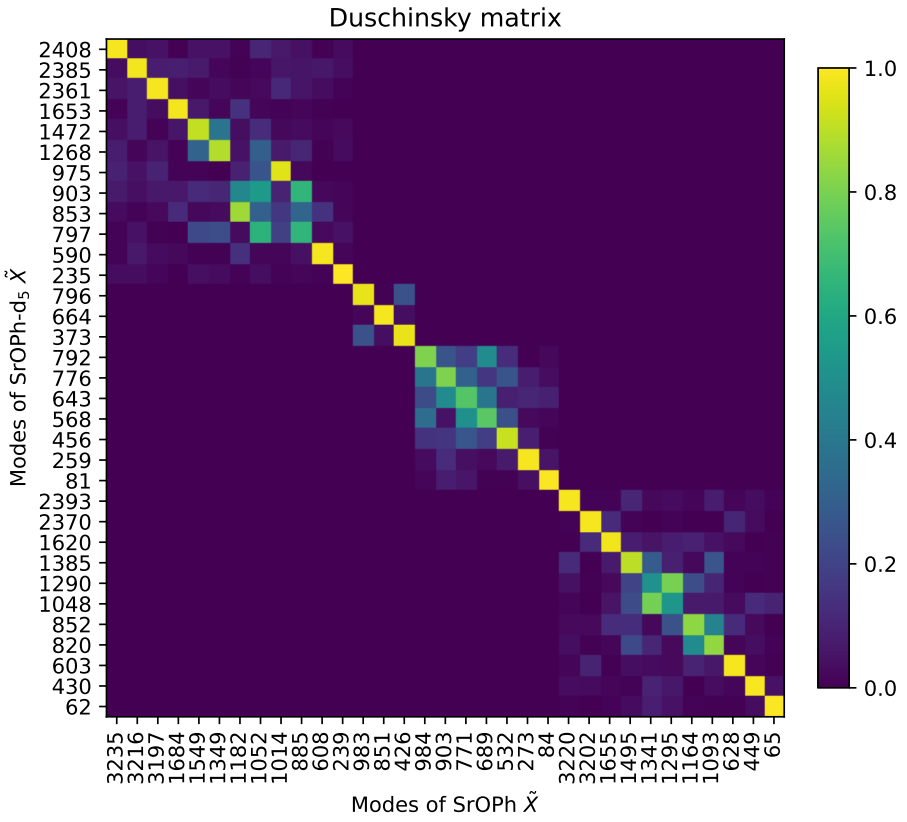


Figure 6: Matrix of inner products between the normal modes of the ground state of SrOPh and its deuterated version SrOPh-$d_5$. Column and row labels show mode frequencies in $cm^{-1}$.

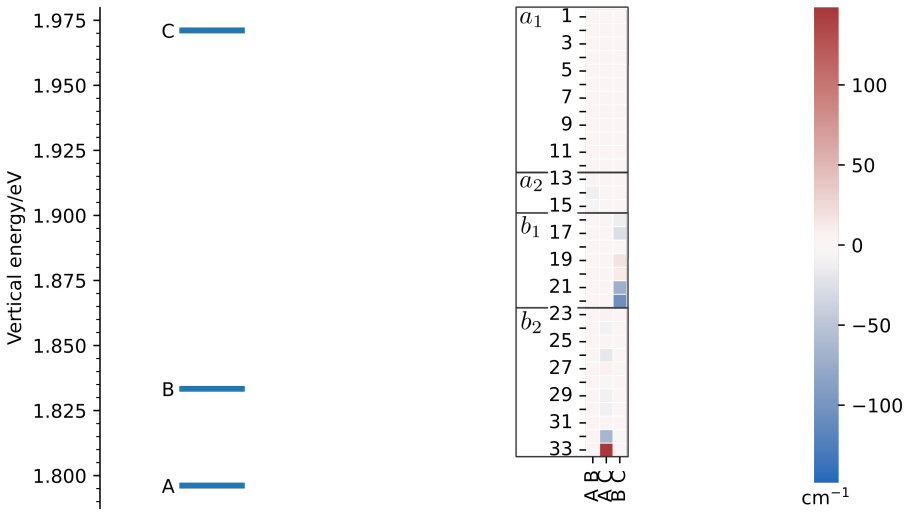


Figure 7: Diabatic couplings for SrOPh-$d_5$, compare to figure 1.

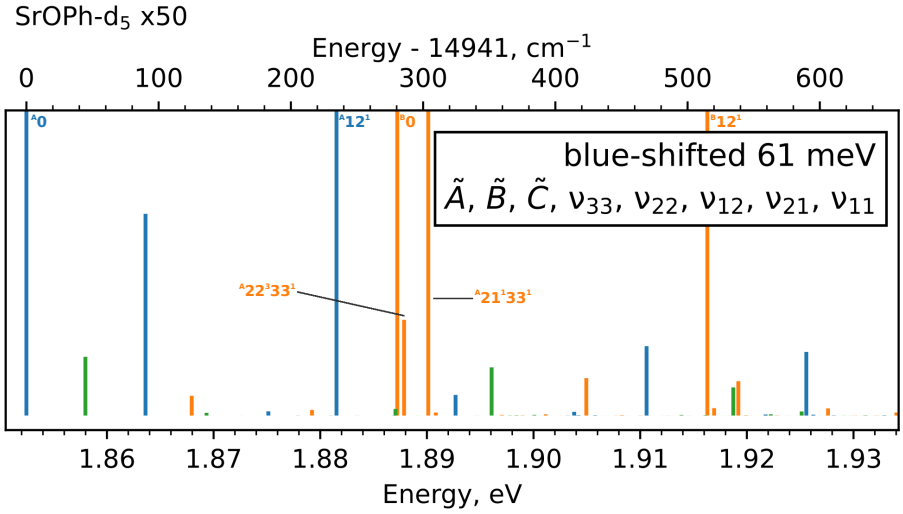


Figure 8: Vibronic absorption spectrum of SrOPh-$d_5$, compare with the undeuterated spectrum from figure 4. Annotations mark the peaks discussed in Sec. 3.2.3.

closer to the bright $^{\tilde{B}}0$ peak.

# 4 Summary

The vibronic effects present in strontium phenoxide make many Franck-Condon-forbidden transitions allowed. Modeling of the vibronic effects in the absorption spectrum of SrOPh using the KDC Hamiltonian in a diabatic basis of Ichino, Gauss, and Stanton reveals that the second order effects lead to significant mixing of the origin band of the $\tilde{B}$ state with the neighbouring states hosted on the $\tilde{A}$ state. These couplings are very sensitive to the exact values of the model parameters such as the vertical excitation energies or harmonic frequencies of the normal modes. The modulation of harmonic frequencies that is afforded by the deuteration of the phenoxide group helps to connect the experimentally observed vibronic features with the modeled couplings scheme.

The *ab initio* calculations show that the vertical excitation energy of the $\tilde{C}$ state is more sensitive to the basis set size and level of correlation than the $\tilde{A}$ and $\tilde{B}$ states.

# References


[1] E. T. Mengesha, A. T. Le, T. C. Steimle, L. Cheng, C. Zhang, B. L. Augenbraun, Z. Lasner, and J. Doyle, "Branching ratios, radiative lifetimes, and transition dipole moments for YbOH", J. Phys. Chem. A **124**, 3135–3148 (2020).

[2] C. Zhang, B. L. Augenbraun, Z. D. Lasner, N. B. Vilas, J. M. Doyle, and L. Cheng, "Accurate prediction and measurement of vibronic branching ratios for laser cooling linear polyatomic molecules", The Journal of Chemical Physics **155**, 091101 (2021).

[3] Z. Lasner, A. Lunstad, C. Zhang, L. Cheng, and J. M. Doyle, "Vibronic branching ratios for nearly closed rapid photon cycling of SrOH", Phys. Rev. A **106**, L020801 (2022).

[4] C. Zhang, N. R. Hutzler, and L. Cheng, "Intensity-borrowing mechanisms pertinent to laser cooling of linear polyatomic molecules", Journal of Chemical Theory and Computation **19**, 4136–4148 (2023).

[5] A. Frenett, Z. Lasner, L. Cheng, and J. M. Doyle, "Vibrational branching fractions for laser cooling of nonlinear strontium-containing molecules", Physical Review A **110**, 022811 (2024).

[6] J. F. Stanton, "On the vibronic level structure in the $NO_3$ radical. I. The ground electronic state", J. Chem. Phys. **126**, 134309–132328 (2007).

[7] H. Köppel, M. Döscher, I. Baldea, H.-D. Meyer, and P. G. Szalay, "Multistate vibronic interactions in the benzene radical cation. II. Quantum dynamical simulations", J. Chem. Phys. **117**, 2657–2671 (2002).

[8] P. Wójcik, H. Reisler, P. G. Szalay, A. I. Krylov, and J. F. Stanton, "Vibronic coupling effects in the photoelectron spectrum of ozone: a coupled-cluster approach", J. Phys. Chem. A **128**, 10957–10964 (2024).

[9] R. Bartlett and M. Musiał, "Coupled-cluster theory in quantum mechanics", Rev. Mod. Phys. **79**, 291–352 (2007).

[10] A. I. Krylov, "Equation-of-motion coupled-cluster methods for open-shell and electronically excited species: The hitchhiker's guide to Fock space", Annu. Rev. Phys. Chem. **59**, 433–462 (2008).

[11] I. Shavitt and R. J. Bartlett, in *Many-body methods in chemistry and physics: MBPT and coupled-cluster theory* (Cambridge University Press, Cambridge, 2009).

[12] K. Sneskov and O. Christiansen, "Excited state coupled cluster methods", WIREs: Comput. Mol. Sci. **2**, 566–584 (2012).

[13] R. J. Bartlett, "Coupled-cluster theory and its equation-of-motion extensions", WIREs: Comput. Mol. Sci. **2**, 126–138 (2012).

[14] A. I. Krylov, "The quantum chemistry of open-shell species", in *Reviews in comp. chem.* Vol. 30, edited by A. L. Parrill and K. B. Lipkowitz (J. Wiley & Sons, 2017), pp. 151–224.

[15] J. Stanton and J. Gauss, "A simple correction to final state energies of doublet radicals described by equation-of-motion coupled cluster theory in the singles and doubles approximation", Theor. Chim. Acta **93**, 303 (1996).

[16] J.F. Stanton, J. Gauss, M.E. Harding, and P.G. Szalay, *CFOUR*, with contributions from A.A. Auer, R.J. Bartlett, U. Benedikt, C. Berger, D.E. Bernholdt, Y.J. Bomble, L. Cheng, O. Christiansen, M. Heckert, O. Heun, C. Huber, T.-C. Jagau, D. Jonsson, J. Jusélius, K. Klein, W.J. Lauderdale, F. Lipparini, D.A. Matthews, T. Metzroth, L.A. Mück, D.P. O'Neill, D.R. Price, E. Prochnow, C. Puzzarini, K. Ruud, F. Schiffmann, W. Schwalbach, C. Simmons, S. Stopkowicz, A. Tajti, J. Vázquez, F. Wang, J.D. Watts; and the integral packages MOLECULE (J. Almlöf and P.R. Taylor), PROPS (P.R. Taylor), ABACUS (T. Helgaker, H.J.Aa. Jensen, P. Jørgensen, and J. Olsen), and ECP routines by A.V. Mitin and C. van Wüllen. For the current version, see http://www.cfour.de.

[17] D. A. Matthews, L. Cheng, M. E. Harding, F. Lipparini, S. Stopkowicz, T.-C. Jagau, P. G. Szalay, J. Gauss, and J. F. Stanton, "Coupled-cluster techniques for computational chemistry: the CFOUR program package", J. Chem. Phys. **152**, 214108 (2020).

[18] A. I. Krylov and P. M. W. Gill, "Q-Chem: An engine for innovation", WIREs: Comput. Mol. Sci. **3**, 317–326 (2013).

[19] E. Epifanovsky, A. T. B. Gilbert, X. Feng, J. Lee, Y. Mao, N. Mardirossian, P. Pokhilko, A. F. White, M. P. Coons, A. L. Dempwolff, Z. Gan, D. Hait, P. R. Horn, L. D. Jacobson, I. Kaliman, J. Kussmann, A. W. Lange, K. U. Lao, D. S. Levine, J. Liu, S. C. McKenzie, A. F. Morrison, K. D. Nanda, F. Plasser, D. R. Rehn, M. L. Vidal, Z.-Q. You, Y. Zhu, B. Alam, B. J. Albrecht, A. Aldossary, E. Alguire, J. H. Andersen, V. Athavale, D. Barton, K. Begam, A. Behn, N. Bellonzi, Y. A. Bernard, E. J. Berquist, H. G. A. Burton, A. Carreras, K. Carter-Fenk, R. Chakraborty, A. D. Chien, K. D. Closser, V. Cofer-Shabica, S. Dasgupta, M. de Wergifosse, J. Deng, M. Diedenhofen, H. Do, S. Ehlert, P.-T. Fang, S. Fatehi, Q. Feng, T. Friedhoff, J. Gayvert, Q. Ge, G. Gidofalvi, M. Goldey, J. Gomes, C. E. González-Espinoza, S. Gulania, A. O. Gunina, M. W. D. Hanson-Heine, P. H. P. Harbach, A. Hauser, M. F. Herbst, M. Hernández Vera, M. Hodecker, Z. C. Holden, S. Houck, X. Huang, K. Hui, B. C. Huynh, M. Ivanov, Á. Jász, H. Ji, H. Jiang, B. Kaduk, S. Kähler, K. Khistyaev, J. Kim, G. Kis, P. Klunzinger, Z. Koczor-Benda, J. H. Koh, D. Kosenkov, L. Koulias, T. Kowalczyk, C. M. Krauter, K. Kue, A. Kunitsa, T. Kus, I. Ladjánszki, A. Landau, K. V. Lawler, D. Lefrancois, S. Lehtola, R. R. Li, Y.-P. Li, J. Liang, M. Liebenthal, H.-H. Lin, Y.-S. Lin, F. Liu, K.-Y. Liu, M. Loipersberger, A. Luenser, A. Manjanath, P. Manohar, E. Mansoor, S. F. Manzer, S.-P. Mao, A. V. Marenich, T. Markovich, S. Mason, S. A. Maurer, P. F. McLaughlin, M. F. S. J. Menger, J.-M. Mewes, S. A. Mewes, P. Morgante, J. W. Mullinax, K. J. Oosterbaan, G. Paran, A. C. Paul, S. K. Paul, F. Pavošević, Z. Pei, S. Prager, E. I. Proynov, Á. Rák, E.

Ramos-Cordoba, B. Rana, A. E. Rask, A. Rettig, R. M. Richard, F. Rob, E. Rossomme, T. Scheele, M. Scheurer, M. Schneider, N. Sergueev, S. M. Sharada, W. Skomorowski, D. W. Small, C. J. Stein, Y.-C. Su, E. J. Sundstrom, Z. Tao, J. Thirman, G. J. Tornai, T. Tsuchimochi, N. M. Tubman, S. P. Veccham, O. Vydrov, J. Wenzel, J. Witte, A. Yamada, K. Yao, S. Yeganeh, S. R. Yost, A. Zech, I. Y. Zhang, X. Zhang, Y. Zhang, D. Zuev, A. Aspuru-Guzik, A. T. Bell, N. A. Besley, K. B. Bravaya, B. R. Brooks, D. Casanova, J.-D. Chai, S. Coriani, C. J. Cramer, G. Cserey, A. E. DePrince, R. A. DiStasio, A. Dreuw, B. D. Dunietz, T. R. Furlani, W. A. Goddard, S. Hammes-Schiffer, T. Head-Gordon, W. J. Hehre, C.-P. Hsu, T.-C. Jagau, Y. Jung, A. Klamt, J. Kong, D. S. Lambrecht, W. Liang, N. J. Mayhall, C. W. McCurdy, J. B. Neaton, C. Ochsenfeld, J. A. Parkhill, R. Peverati, V. A. Rassolov, Y. Shao, L. V. Slipchenko, T. Stauch, R. P. Steele, J. E. Subotnik, A. J. W. Thom, A. Tkatchenko, D. G. Truhlar, T. Van Voorhis, T. A. Wesolowski, K. B. Whaley, H. L. Woodcock, P. M. Zimmerman, S. Faraji, P. M. W. Gill, M. Head-Gordon, J. M. Herbert, and A. I. Krylov, "Software for the frontiers of quantum chemistry: An overview of developments in the Q-Chem 5 package", J. Chem. Phys. **155**, 084801 (2021).

[20] H. Köppel, W. Domcke, and L. Cederbaum, "Multimode molecular dynamics beyond the Born–Oppenheimer approximation", Adv. Chem. Phys. **57**, 59 (1984).

[21] W. Domcke, H. Köppel, and L. S. Cederbaum, "Spectroscopic effects of conical intersections of molecular potential energy surfaces", Mol. Phys. **43**, 851–875 (1981).

[22] H. Köppel, W. Domcke, and L. S. Cederbaum, "The multi-mode vibronic-coupling approach", in *Conical intersections*, edited by W. Domcke, D. R. Yarkony, and H. Köppel (World Scientific Publ Co Pte Ltd, 2004) Chap. 7, pp. 323–367.

[23] T. Ichino, J. Gauss, and J. F. Stanton, "Quasidiabatic states described by coupled-cluster theory", J. Chem. Phys. **130**, 174105 (2009).

[24] J. F. Stanton and J. Gauss, "Analytic energy gradients for the equation-of-motion coupled-cluster method: Implementation and application to the HCN/HNC system", J. Chem. Phys. **100**, 4695–4698 (1994).

[25] K. Sharma, O. A. Vasilyev, T. A. Miller, and J. F. Stanton, "Molecules with spin and vibronic coupling effects: a computational perspective", in Journal of physics: conference series, Vol. 2769, 1 (IOP Publishing, 2024), p. 012002.

[26] T. Khvorost, P. Wójcik, C. Chang, M. Calvillo, C. Dickerson, A. I. Krylov, and A. N. Alexandrova, "Dual optical cycling centers mounted on an organic scaffold: new insights from quantum chemistry calculations and symmetry analysis", J. Phys. Chem. Lett. **15**, 5665–5673 (2024).

[27] R. S. Mulliken, "Report on notation for the spectra of polyatomic molecules", J. Chem. Phys. **23**, 1997–2011 (1955).

[28] N. H. Pilgram, "Production and Characterization of Ytterbium Monohydroxide (YbOH) for Next-Generation Parity and Time-Reversal Violating Physics Searches", PhD thesis (California Institute of Technology, Pasadena, California, Aug. 4, 2022), 261 pp.

[29] B. L. Augenbraun, S. Burchesky, A. Winnicki, and J. M. Doyle, "High-resolution laser spectroscopy of a functionalized aromatic molecule", J. Phys. Chem. Lett. **13**, 10771–10777 (2022).